Triply periodic surfaces and multiply continuous structures from the Landau model of microemulsions

Wojciech T. Góźdź and Robert Hołyst
Institute of Physical Chemistry, Polish Academy of Sciences, Kasprzaka 44/52, 01-224 Warsaw, Poland
(Received 26 April 1996)

We present a method for the generation of periodic embedded surfaces of nonpositive Gaussian curvature and multiply continuous phases. The structures are related to the local minima of the scalar order parameter Landau-Ginzburg Hamiltonian for microemulsions. In the bicontinuous structure the single surface separates the volume into two disjoint subvolumes. In some of our phases (multiply continuous) there is more than one periodic surface that disconnects the volume into three or more disjoint subvolumes. We show that some of these surfaces are triply periodic minimal surfaces. We have generated known minimal surfaces (e.g., Schwarz primitive P, diamond D, and Schoen-Luzatti gyroid G and many surfaces of high genus. We speculate that the structure of microemulsion can be related to the high-genus gyroid structures, since the high-genus surfaces were most easily generated in the phase diagram close to the microemulsion stability region. We study in detail the geometrical characteristics of these phases, such as genus per unit cell, surface area per unit volume, and volume fraction occupied by oil or water in such a structure. Our discovery calls for new experimental techniques, which could be used to discern between bicontinuous and multiply continuous structures. We observe that multiply continuous structures are most easily generated close to the water-oil coexistence region. [S1063-651X(96)01311-6]

PACS number(s): 61.20.−p, 64.75.+g, 68.10.−m, 02.40.−k

I. INTRODUCTION: MICROEMULSION

Amphiphilic molecules are composed of two different parts: a hydrophobic tail and a hydrophilic head. The tail is composed of one or more hydrocarbon chains, usually with 6–20 carbon atoms; the head is composed of chemical groups of high affinity to water [1,2]. Such a composition of amphiphilic molecules results in many amazing properties of systems containing these molecules. Adding an appropriate amount of amphiphile to a mixture of oil and water, two liquids that are immiscible under normal conditions, causes complete mixing of these liquids. The amount of amphiphile necessary to cause mixing depends on the strength of the amphiphile. The longer the hydrocarbon chain the stronger the amphiphile. The strength of the amphiphile similarly depends on the number of hydrophilic groups in the amphiphilic molecule. Complete mixing is enabled by lowering the oil-water surface tension by the amphiphile. That is why the amphiphilic molecules are also called surfactants: surface active agents. The surfactant assembles at the interface, forming a monolayer, in such a way that the hydrophilic part of the amphiphile is located in water and the hydrophobic part in oil. The surfactant monolayer separates coherent regions of oil and water. Usually the monolayer width is small compared to the size of oil and water regions unless the concentration of surfactant is very high. In such a situation the formation of water and oil droplets suspended in the surfactant solution is possible. Surfactants dissolved in water can form micells of different shape: spherical or cylindrical. They can also assemble into bilayers grouping the hydrophobic part of the surfactant inside the bilayer. Such a system is called the sponge phase.

When comparable amounts of oil and water are mixed with the surfactant a new homogeneous, isotropic, thermodynamically stable phase is created [3]. This phase, called microemulsion, can coexist with oil and water [4,1,2]. The measurements of electrical conductivity, self-diffusion, NMR, and freeze fracture microscopy studies indicate that the structure of microemulsion is bicontinuous [5,6,1,7,8]. That is, the microemulsion is composed of water and oil channels mutually interwoven, separated by the monolayer of surfactant. The amphiphilic systems can form apart from the structured disordered phase like microemulsion, many-ordered phases. The most common are the lamellar and hexagonal. The lamellar phase is composed of the regions of water and oil separated by the surfactant monolayer. The lamellar phase looks like a sandwich composed of the slices of water and oil separated by a monolayer of surfactant. The hexagonal phase is composed of cylinders of water or oil bounded by the layer of surfactant, arranged on a hexagonal lattice, immersed in oil or water. The most interesting are the ordered cubic bicontinuous phases. The most prominent examples are the gyroid, double diamond (sometimes called diamond) [9], and simple cubic phase.

The systems containing surfactants are difficult to characterize. They are structured liquid ternary mixtures. For example, microemulsion on a macroscopic level looks like an ordinary homogeneous fluid. However, it is known that the microemulsion is composed of three components: two of them, oil and water, do not mix in the absence of the third one, the surfactant. Thus the presence of the surfactant is crucial. It is obvious that information about the location of surfactant in its mixtures characterizes the mixtures in the best way. The surfactant forms a monolayer at the water-oil interface. This monolayer can be approximated in the theory by a mathematical surface. Thus, in order to characterize the systems containing surfactants it is enough to characterize this surface and its properties such as the surface area, genus, and its curvatures [10–14].

There are three levels of description of these mixtures: macroscopic, mesoscopic, and microscopic. Here we concentrate on the mesoscopic level, described by the Landau-Ginzburg theory developed recently. We note that the most interesting phenomena take place on the mesoscopic scale, which is intermediate between the microscopic and macroscopic. The typical sizes of oil-rich domains in the mixture are often 1000 Å, which is much larger than the size of a surfactant (25 Å), but much smaller than the macroscopic scale of millimeters [1]. This means that microemulsion is structured on the mesoscopic scale, which justifies the choice of the Landau-Ginzburg model for its descriptions. In the next section we describe the Landau-Ginzburg theory that we use to generate the surfaces in the oil, water, and surfactant mixtures.

The paper is arranged as follows. In Sec. II we describe the Landau-Ginzburg functional used in our calculations. Section III describes numerical procedure used to solve the functional. In Sec. IV we present the results.

II. LANDAU-GINZBURG MODEL

The theoretical model describing the behavior of the system containing surfactants originates from the expansion in gradients of the Landau-Ginzburg free energy [15]:

$$\begin{aligned}\mathcal{F}[\phi(\mathbf{r})]=\int d^3\mathbf{r}[&a_0+a_1\phi(\mathbf{r})+a_2\phi(\mathbf{r})^2+a_3\phi(\mathbf{r})^3\\&+a_4\phi(\mathbf{r})^4+a_5\phi(\mathbf{r})^5+a_6\phi(\mathbf{r})^6+\cdots\\&+c_1|\nabla\phi(\mathbf{r})|^2+c_2|\Delta\phi(\mathbf{r})|^2+\cdots\\&+\phi(\mathbf{r})^2|\nabla\phi(\mathbf{r})|^2+\cdots].\end{aligned}\tag{1}$$

This is the simplest model with a single scalar order parameter $\phi(\mathbf{r})$. The analysis of (1) shows that the essential features of systems with internal interfaces can be recovered by keeping $c_1<0$ and $c_2>0$. The gradient term with negative coefficient c_1 tends to create the interface, whereas the Laplacian term with the positive coefficient c_2 stabilizes the system. The number of terms and the values of coefficients in the expansion of the scalar order parameter $\phi(\mathbf{r})$ in power series depends on the problem to be studied. In order to study microemulsion and ordered phases that appear in systems containing surfactants the following Landau-Ginzburg functional was proposed [16,17] based on (1):

$$\begin{aligned}\mathcal{F}[\phi(\mathbf{r})]=\int d^3\mathbf{r}[&c|\Delta\phi(\mathbf{r})|^2+g(\phi(\mathbf{r}))|\nabla\phi(\mathbf{r})|^2+f(\phi(\mathbf{r}))\\&+\mu\phi(\mathbf{r})].\end{aligned}\tag{2}$$

We have used in our calculations the model (2) with the functions $g(\phi(\mathbf{r}))$ and $f(\phi(\mathbf{r}))$ given by

$$g(\phi(\mathbf{r}))=g_2\phi(\mathbf{r})^2+g_0,\tag{3}$$

$$f(\phi(\mathbf{r}))=\omega[\phi(\mathbf{r})+\phi_w]^2[\phi(\mathbf{r})^2+f_0][\phi(\mathbf{r})+\phi_o]^2,\tag{4}$$

and the set of constants $\phi_o=-\phi_w=1$, $c=1$, $\omega=1$, and $\mu=0$.

The values of the field $\phi(\mathbf{r})$ are proportional to the difference in oil and water concentrations and are negative for water and positive for oil regions or vice versa. The sign is just a matter of convention. The surface

$$\phi(\mathbf{r})=0\tag{5}$$

describes the interface between oil and water. The function $f(\phi(\mathbf{r}))$ is the bulk free energy. μ is the chemical potential difference between oil and water. The surfactant degrees of freedom are considered as being integrated out and the surfactant properties enter the functional (2) through the form of the functions $g(\phi(\mathbf{r}))$ and $f(\phi(\mathbf{r}))$. The functional (2) can be used also to model the sponge phase. In such a case the negative values of the order parameter are interpreted as the interior part of the sponge phase and the positive values as the exterior part of the phase (or vice versa).

The function $f(\phi(\mathbf{r}))$ has by construction three minima, which guarantees three phase coexistence, i.e., oil, water, and microemulsion. The minima for oil-rich and water-rich phases are of equal depth, which makes the system symmetric; therefore μ has to be set to zero. Varying the parameter f_0 makes the middle phase (microemulsion) more or less stable with respect to two bulk phases. Thus f_0 is proportional to the chemical potential of microemulsion. The constant g_2 depends on g_0 and f_0 and is chosen in such a way that the correlation function $G(r)=\langle\phi(\mathbf{r})\phi(\mathbf{0})\rangle$ decays monotonically in the oil-rich and water-rich phases [17,5]. Here we take $g_2=4\sqrt{1+f_0}-g_0+0.01$. The more negative g_0 the stronger or more surfactant used.

In the Gaussian approximation the water-water structure factor $S_{ww}(k)$ for (2) is given by

$$S_{ww}(k)\propto\frac{1}{ck^4+g(\phi_b)k^2+\frac{1}{2}f''(\phi_b)},\tag{6}$$

$\phi_b\in\{\phi_w,\phi_m,\phi_0\}$. For the oil-rich phase $\langle\phi(\mathbf{r})\rangle\simeq\phi_0$, for the water-rich phase $\langle\phi(\mathbf{r})\rangle\simeq\phi_w$, and for microemulsion $\langle\phi(\mathbf{r})\rangle\simeq\phi_m=0$. A peak at $k>0$ (for $\phi_b=\phi_m$) indicates a local structure of microemulsion with characteristic size $\xi\sim2\pi/k$. For $\phi_b=\phi_0$ or ϕ_w the structure factor has a peak only at $k=0$, indicating that pure oil and water phases behave like a normal liquid with no internal structure. The water-water structure factor $S_{ww}(k)$ can be measured in experiments. Thus the quality of the theory can be checked out by comparing theoretical predictions with an experiment. It turns out that (6) describes extremely well the data from the scattering experiments [16,7]. The model (2) has been successfully used to describe the wetting behavior of the microemulsion at the oil-water interface [17–20] to investigate a few ordered phases such as lamellar, double diamond, simple cubic, hexagonal, or crystals of spherical micells [21,22] and to study the mixtures containing surfactant in a confined geometry [23].

An enormous advantage of the model (2) is its simplicity. It is extraordinary that the properties of a very complex system are described by the one scalar order parameter field. There are a few Landau-Ginzburg theories with more than one order parameter field [5,24–28]. However, adding a new order parameter field does not automatically make the model better. It does, for sure, make solving the model more difficult and it involves the introduction of new parameters, the physical meaning of which is not always clear.

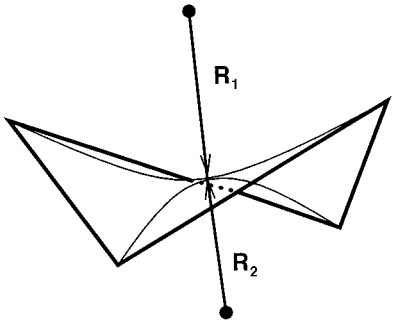

FIG. 1. Piece of surface with nonpositive Gaussian curvature. R_1 and R_2 are the principal radii. The Gaussian (K) and the mean (H) curvatures are expressed in terms of the principal radii as $H=1/2R_1+1/2R_2$ and $K=1/R_1R_2$. If $R_1=-R_2$ at every point, the surface is called minimal. This implies that K is nonpositive at every point.

In the mean-field approximation the stable or metastable phases of the system correspond to the minimum of the functional (2) and the crucial information about the structure is contained in the properties of the surface $\phi(\mathbf{r})=0$ formed, in the system, by surfactant. We have observed [29] the very special property of the functional (2) related to this surface. We have discovered it by analyzing the formula for the mean curvature (Fig. 1) expressed in terms of the three-dimensional field $\phi(\mathbf{r})$. From the form of (2) one can realize that for some local minima of (2) the average curvature given by

$$H(\mathbf{r})=-\frac{1}{2}\nabla\left(\frac{\nabla\phi(\mathbf{r})}{|\nabla\phi(\mathbf{r})|}\right)=-\frac{1}{2}\frac{\Delta\phi(\mathbf{r})}{\nabla\phi(\mathbf{r})|}+\frac{\nabla\phi(\mathbf{r})\nabla|\nabla\phi(\mathbf{r})|}{2|\nabla\phi(\mathbf{r})|^2} \tag{7}$$

vanishes at every point of the $\phi(\mathbf{r})=0$ surface. It follows from the second term of (2) that $|\nabla\phi(\mathbf{r})|$ should have the maximal value for $\phi(\mathbf{r})=0$ (note that $g_0<0$) and consequently the second term (which after a small algebra can be written as $[\partial|\nabla\phi(\mathbf{r})|/\partial n]/2|\nabla\phi(\mathbf{r})|$, with ∂n denoting the derivative along the normal to the surface) in (7) vanishes. Also for the $\phi(\mathbf{r}),-\phi(\mathbf{r})$ symmetry we know that $H(\mathbf{r})$ averaged over the whole surface should be zero. This means that $\Delta\phi(\mathbf{r})$ either is exactly zero at the surface or changes sign. From the first term of (2) it follows that the former is favored and consequently $H(\mathbf{r})=0$ at every point $\mathbf{r}$ at the surface $\phi(\mathbf{r})=0$. The surface such that the mean curvature vanishes at its every point is called minimal. Therefore, before solving (2) we observe that among the local minima of the functional (2) the structures with minimal surfaces should be favored. The argument presented here has a local nature and does not rule out other possibilities.

III. MINIMIZATION OF THE FUNCTIONAL

In order to find the local minima of the functional (2) we have discretized it on the cubic lattice. Thus the functional $\mathcal{F}[\phi(\mathbf{r})]$ becomes a function $F(\{\phi_{i,j,k}\})$ of N^3 variables, where $L=(N-1)h$ is the linear dimension of the cubic lattice, h is the lattice spacing, and $\{\phi_{i,j,k}\}$ stands for the set of all variables of the function. Each variable $\phi_{i,j,k}$ represents the value of the field $\phi(\mathbf{r})$ at the point $\mathbf{r}=(i,j,k)h$ and $i,j,k=1,\ldots,N$. In our calculations we use $N=129$, which results in over 2×10^6 points per unit cell.

All structures we have investigated are periodic. Thus periodicity had to be incorporated into the functional (2). It was done by periodic boundary conditions $\phi_{1,j,k}=\phi_{N,j,k}\phi_{2,j,k}=\phi_{N+1,j,k}$, $\phi_{3,j,k}=\phi_{N+2,j,k}\phi_{0,j,k}=\phi_{N-1,j,k}$, and $\phi_{-1,j,k}=\phi_{N-2,j,k}$, and similarly in the y and z directions. The points outside the unit cell, given by the periodic boundary conditions, enter the functional through the calculations of derivatives of points at the boundary and near the boundary of the lattice, i.e., when at least one of the indices i,j,k is equal to $1,2,N-1,N$.

The first and second derivatives in the gradient and Laplacian term of the functional (2) at the point $\mathbf{r}=(i,j,k)h$ on the lattice were calculated according to the formulas [30]

$$\frac{\partial\phi(\mathbf{r})}{\partial x}\rightarrow\frac{\phi_{i+1,j,k}-\phi_{i-1,j,k}}{2h} \tag{8}$$

and

$$\frac{\partial^2\phi(\mathbf{r})}{\partial x^2}\rightarrow\frac{1}{12h^2}(-\phi_{i+2,j,k}+16\phi_{i+1,j,k}-30\phi_{i,j,k}+16\phi_{i-1,j,k}-\phi_{i-2,j,k}), \tag{9}$$

and similarly in the y and z directions. The mixed derivatives used in (18) and (19) are calculated according to [30]

$$\frac{\partial^2\phi(\mathbf{r})}{\partial x\partial y}\rightarrow-\frac{1}{2h^2}(\phi_{i+1,j,k}+\phi_{i-1,j,k}+\phi_{i,j+1,k}+\phi_{i,j-1,k}-2\phi_{i,j,k}-\phi_{i+1,j+1,k}-\phi_{i-1,j-1,k}). \tag{10}$$

A. Choosing the surface

The order parameter field $\phi(\mathbf{r})$ carries an enormous amount of information about the local structure of the phases we have investigated. The most interesting is the topology of the phases, described by the surface

$$\phi(\mathbf{r}=(x,y,z))=0, \tag{11}$$

dividing positive and negative regions of the order parameter field. Thus it was crucial in our studies to find the location of the surface $\phi(\mathbf{r})=0$.

It is highly unlikely, because of numerical accuracy, that a value of the field $\phi(\mathbf{r})=\phi_{i,j,k}$ at the point $\mathbf{r}=(i,j,k)h$ on the lattice is exactly zero. Therefore the points of the surface have to be localized by interpolation between the neighboring sites of the lattice. If $\phi(\mathbf{r}_1=(i,j,k)h)=\phi_{i,j,k}<0$ and $\phi(\mathbf{r}_2=(i+1,j,k)h)=\phi_{i+1,j,k}>0$, then the point $\mathbf{r}_0$, for which $\phi(\mathbf{r}_0)=0$, must lie between the points $\mathbf{r}_1=(i,j,k)h$ and $\mathbf{r}_2=(i+1,j,k)h$. Moreover, the location of $\mathbf{r}_0$ depends on the values of the field at the points $\mathbf{r}_1$ and $\mathbf{r}_2$ as

$$\mathbf{r}_0=\left(i+\frac{|\phi_{i,j,k}|}{|\phi_{i,j,k}-\phi_{i+1,j,k}|},j,k\right)h. \tag{12}$$

B. Triangulation, surface area, and volume

In the way described in the preceding section, one can find the points of the surface $\phi(\mathbf{r})=0$ located between the

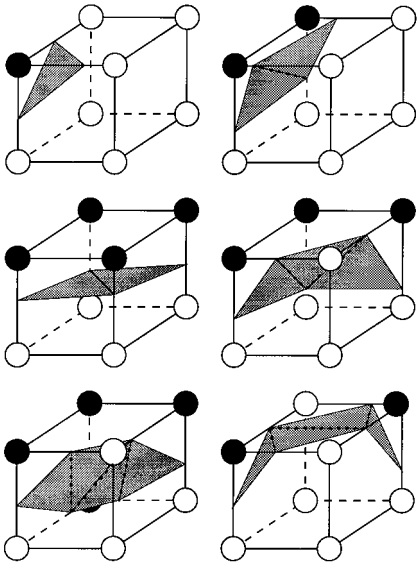

FIG. 2. Possible configurations of passing the surface $\phi(\mathbf{r})=0$ through the field $\phi(\mathbf{r})$ discretized on the lattice. Black circles represent $\phi_{i,j,k}<0$, whereas white circles $\phi_{i,j,k}>0$. The cubes represent the smallest pieces of the lattice of linear dimension h. For smooth surfaces studied here cases of 3–6 vertices of the surface in a small cube are the only cases. Cases of 7–9 and 12 vertices in a single cube have not been encountered.

neighboring lattice sites. However, this is not enough to describe the surface. It is also necessary to specify the connections between these points to characterize the surface.

Due to discretization the unit cell is divided on $(N-1)^3$ small cubes of the size of the lattice spacing h. The surface $\phi(\mathbf{r})=0$ passing through a small cube cuts out of it a polygon, whose edges are formed by the intersection of the surface and faces of the small cube. The edges of the polygon can be approximated by straight lines. The possible configurations of the surface $\phi(\mathbf{r})=0$ cutting a small cube are pictured in Fig. 2. The surface $\phi(\mathbf{r})=0$ can cut out only four kinds of polygons: a triangle, a tetragon, a pentagon, and a hexagon. The edges of these polygons, except the triangle, do not lie in a common plane. It is necessary to specify also the connections between the vertices of the polygon, to characterize the surface unambiguously. This was done in the way shown in Fig. 2, with thick dotted lines in the patches of the surface inside the small cubes. This procedure makes the surface covered only with triangles. The triangulation described above was used to calculate the surface area inside a unit cell by summing up the surface area of all triangles.

The triangulation was also used to calculate the volume ratio of the two subvolumes. The surface $\phi(\mathbf{r})=0$ separates the volume of a given phase into two subvolumes, first occupied by the field $\phi(\mathbf{r})>0$ and second by $\phi(\mathbf{r})<0$. In order to calculate the volume occupied by the negative or positive values of the field $\phi(\mathbf{r})$ the volume of the small cubes not cut by the surface $\phi(\mathbf{r})=0$ is calculated. Next we use the triangulated surface $\phi(\mathbf{r})=0$ to divide the small cubes with the values of the field $\phi(\mathbf{r})$ of different sign at the vertices. The surface $\phi(\mathbf{r})=0$ divides a small cube into two polyhedra. The volumes of these polyhedra for negative and positive values of the field $\phi(\mathbf{r})$ were calculated and added to the previously calculated volume for regions of positive and negative values of $\phi(\mathbf{r})$.

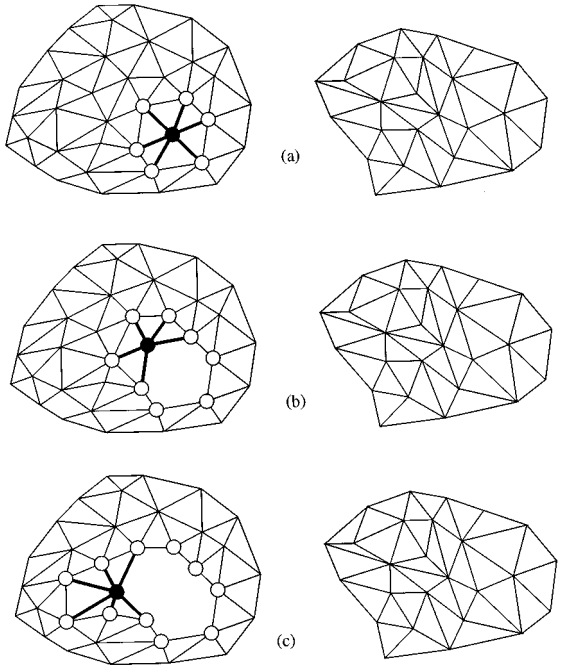

FIG. 3. Schematic illustration of the separation of two disjoint surfaces.

For more than one periodic surface, in the unit cell, it is necessary to separate different surfaces to be able to calculate the surface area and genus of each surface. In order to find the points that belong to the same surface one has to choose an arbitrary point on one of the surfaces and follow the connections between points to find the rest of the points belonging to this surface. The set of connections will uniquely specify the surface. Figure 3 illustrates the way this process can be done for two surfaces. Having chosen an arbitrary point on one surface, represented by a black circle in Fig. 3(a), one has to find among all the connections between couples of points specified by the triangulation the connections including this point. They are represented by thick solid lines connecting the black circle with the white circles. Next one has to chose arbitrarily a point among the points represented by white circles and find all connections between this point and the points remaining after removing from the set of connections the connections containing the first point. This is shown in Fig. 3(b). Such a procedure has to be repeated until no more than one point represented by the white circle is left.

C. Euler characteristics and genus

The triangulation can also be used to calculate the Euler characteristics χ of the surface inside the unit cell. The calculation of χ can be done according to the Euler formula [31]

$$\chi=F+V-E, \tag{13}$$

where F,V,E are the numbers of faces (F), vertices (V), and edges (E) of the polygons cut out by the surface $\phi(\mathbf{r})=0$ in the small cubes of dimension of lattice spacing (Fig. 3). The fact that each polygon is inside a small cube makes the cal-

culation very easy because each vertex of the polygon belongs to four polygons since it lies on the edge of the small cube. Therefore, to calculate χ one does not need to know the connections between points. It is sufficient to know only how many times the surface $\phi(\mathbf{r})=0$ cuts the edges of the small cube and how many cubes it cuts. The number of faces (F) is therefore the number of small cubes cut by the surface $\phi(\mathbf{r})=0$, that is, the cubes with the values of the field $\phi(\mathbf{r})=\phi_{i,j,k}$ of different sign at its vertices. The number of vertices is given by the number of intersections of the surface $\phi(\mathbf{r})=0$ with the edges of the small cubs taken with a weight $\frac{1}{4}$ because each edge belongs to four cubes. The number of edges (E) is the same as the number of vertices, but it has to be taken with a weight $\frac{1}{2}$ because the polygon edges lie in the faces of small cubes and each face belongs to two cubes. Only the last case shown in Fig. 2 needs a slightly different treatment since one face of the surface lies on the face of the small cube.

The Euler characteristic for the closed surface is related to the Gaussian (K) curvature and genus (g) of this surface as [31,32]

$$\chi=\frac{1}{2\pi}\int_S K\,dS=2(1-g), \tag{14}$$

where the integral is taken over the surface S. The genus is an integer number and tells how many holes are in a closed surface. For example, the genus for a sphere is zero, for a torus one, and for a pretzel is two. The structures we have investigated are infinite and periodic. The genus for an infinite surface is infinite, of course, but for a finite piece of this surface, in a unit cell, it is finite and characterizes the surface. Due to periodicity the unit cubic cell can be treated as a closed surface in four dimensions, making the calculation of the genus for the infinite periodic surface fully justified [33]. Therefore, the genera of the structures were calculated according to $g=1-\chi/2$, where χ is the Euler characteristic for the surface inside a unit cell.

D. Curvatures

The Gaussian and the mean curvatures present another characteristic of the internal surfaces given by $\phi(\mathbf{r})=0$. In the description of the model we have mentioned that some of the structures in the model should be characterized by zero mean curvature at every point of the internal interface. Here we present the method used to compute Gaussian and mean curvatures. The unit normal $\mathbf{n}(\mathbf{r})$ at the point $\mathbf{r}$ is given by the gradient of the field $\phi(\mathbf{r})$,

$$\mathbf{n}(\mathbf{r})=\frac{\nabla\phi(\mathbf{r})}{|\nabla\phi(\mathbf{r})|}. \tag{15}$$

The mean (H) curvatures is given by the divergence of the unit vector [34], normal to the surface at the point $\mathbf{r}$, $\mathbf{n}(\mathbf{r})$,

$$H(\mathbf{r})=-\frac{1}{2}\nabla\mathbf{n}(\mathbf{r})=-\frac{1}{2}\nabla\frac{\nabla\phi(\mathbf{r})}{|\nabla\phi(\mathbf{r})|} \tag{16}$$

and the Gaussian curvature (K) by the formula [35]

$$K(\mathbf{r})=\tfrac{1}{2}\{-(\partial_i n_j)^2+[\nabla\mathbf{n}(\mathbf{r})]^2\}. \tag{17}$$

In numerical calculations of the curvatures we used the formulas [34,36]

$$H=-\frac{1}{2\sqrt{\phi_x^2+\phi_y^2+\phi_z^2}}\frac{B}{A}, \tag{18}$$

$$K=\frac{1}{\phi_x^2+\phi_y^2+\phi_z^2}\frac{C}{A}, \tag{19}$$

where A, B, and C are obtained from

$$\det\begin{pmatrix}(\phi_{xx}-\lambda) & \phi_{xy} & \phi_{xz} & \phi_x\\ \phi_{yx} & (\phi_{yy}-\lambda) & \phi_{yz} & \phi_y\\ \phi_{zx} & \phi_{zy} & (\phi_{zz}-\lambda) & \phi_z\\ \phi_x & \phi_y & \phi_z & 0\end{pmatrix}=A\lambda^2+B\lambda+C \tag{20}$$

and are given by

$$A=-(\phi_x^2+\phi_y^2+\phi_z^2), \tag{21}$$

$$B=\phi_x^2(\phi_{yy}+\phi_{zz})+\phi_y^2(\phi_{xx}+\phi_{zz})+\phi_z^2(\phi_{xx}+\phi_{yy})-2\phi_x\phi_y\phi_{xy}-2\phi_x\phi_z\phi_{xz}-2\phi_y\phi_z\phi_{yz}, \tag{22}$$

$$C=\phi_x^2(\phi_{yz}^2-\phi_{yy}\phi_{zz})+\phi_y^2(\phi_{xz}^2-\phi_{xx}\phi_{zz})+\phi_z^2(\phi_{xy}^2-\phi_{xx}\phi_{yy})+2\phi_x\phi_z(\phi_{xz}\phi_{yy}-\phi_{xy}\phi_{yz})+2\phi_x\phi_y(\phi_{xy}\phi_{zz}-\phi_{xz}\phi_{yz})+2\phi_y\phi_z(\phi_{yz}\phi_{xx}-\phi_{xy}\phi_{xz}). \tag{23}$$

The mean and Gaussian curvatures have to be computed at the points of the surface $\phi(\mathbf{r})=0$. These points do not lie exactly at the lattice sites. In order to calculate the derivatives of the field $\phi(\mathbf{r})$ at the point $\mathbf{r}_0$, for which $\phi(\mathbf{r}_0)=0$, according to the formulas (8)–(10) the values of the field $\phi(\mathbf{r})$ at the points $\mathbf{r}_0+(0,0,h)$, $\mathbf{r}_0+(0,h,0)$, $\mathbf{r}_0+(h,0,0)$, $\mathbf{r}_0+(0,0,2h)$, $\mathbf{r}_0+(0,2h,0)$, $\mathbf{r}_0+(2h,0,0)$, $\mathbf{r}_0+(0,h,h)$, $\mathbf{r}_0+(h,h,0)$, and $\mathbf{r}_0+(h,0,h)$ have to be interpolated. The point $\mathbf{r}_0$ is $|\phi_{i,j,k}|/|\phi_{i,j,k}-\phi_{i,j+1,k}|=\Delta h$ away from the point $\mathbf{r}=(i,j,k)h$. Then the value of the field $\phi(\mathbf{r})$ at, e.g., the point $\mathbf{r}_0+(0,h,0)$ is $\Delta h(\phi_{i,j+1,k}-\phi_{i,j,k})$. The values of the field $\phi(\mathbf{r})$ in the remaining points can be calculated in a similar way.

E. Building an initial configuration

The minimization procedure always requires an initial configuration. Here we present the initial configurations used in minimization of structures of different symmetries.

The initial configuration is set up by building the field $\phi(\mathbf{r})$ for a unit cell first on a small cubic lattice, $N=3$ or 5, analogously to a two-component AB molecular crystal. The value of the field $\phi(\mathbf{r})=\phi_{i,j,k}$ at the point $\mathbf{r}=(i,j,k)h$ on the lattice is set to 1 if in the molecular crystal an atom A is in this place; if there is an atom B, $\phi_{i,j,k}$ is set to -1; if there is an empty place $\phi_{i,j,k}$ is set to 0. Figure 4(a) shows the initial configuration used to build the field $\phi(\mathbf{r})$ for the simple cubic phase unit cell. Filled black circles represent atoms of type A and hollow circles represent atoms of type B. In this case all

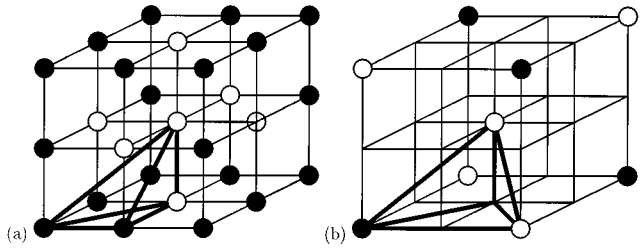

FIG. 4. Initial configuration used to create structures of symmetry of (a) the simple cubic phase and (b) the double diamond phase.

sites are occupied by atoms A or B. Figure 4(a) shows the initial configuration used to build the field $\phi(\mathbf{r})$ for the double diamond phase in $\frac{1}{8}$ of the unit cell. There are unoccupied sites in this case and in these sites the value of the field $\phi(\mathbf{r})=\phi_{i,j,k}$ is set to zero. It would be difficult to present the initial configuration for the gyroid phase because it would require drawing the picture of lattice of size $N=9$. Such a picture would be unreadable. Therefore we present this configuration schematically in Fig. 5(a). The solid and dotted lines show the channels of oil and water. The thick dashed lines show the region occupied by a rectangular parallelopiped used to build the unit cell. The fractions represent the value of the z coordinate of an atom in the unit cell. In order to better visualize this configuration we present in Fig. 5(b) the points on the lattice, in a unit cell, with the values of the field $\phi(\mathbf{r})$ set initially to -1 (light gray spheres) and $+1$ (dark gray spheres).

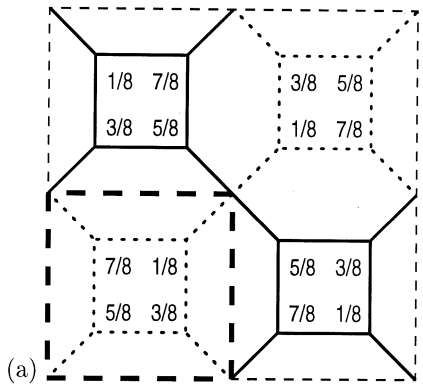

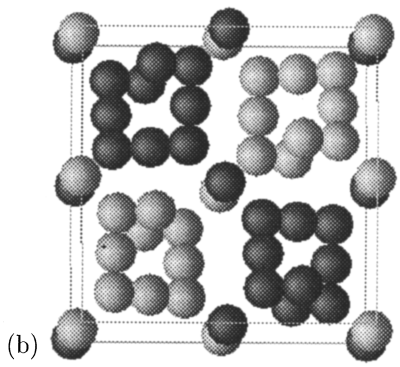

FIG. 5. Initial configuration used to create structures of symmetry of gyroid phase: (a) schematic representation and (b) field representation.

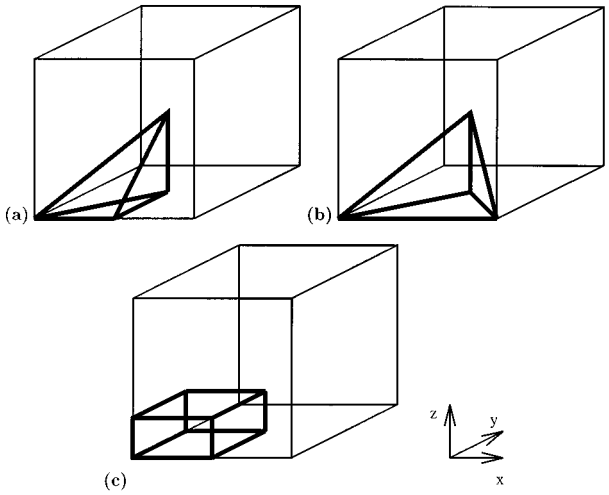

FIG. 6. Thick solid lines show the kaleidoscopic cell used to create (a) the unit cell for the structures of simple cubic phase symmetry (the quadrirectangular tetrahedron is the kaleidoscopic cell) [see Fig. 4(a)], (b) $\frac{1}{8}$ of the unit cell for the structures of double diamond symmetry (the trirectangular tetrahedron is the kaleidoscopic cell) [see Fig. 4(b)] and (c) the unit cell for the structures of gyroid phase symmetry (the rectangular parallelopiped is the kaleidoscopic cell) (see Fig. 5).

The tetrahedrons drawn in Figs. 4(a) and 4(b) with thick solid lines are the kaleidoscopic cells used to build the unit cell. The way of constructing the unit cell by replicating the kaleidoscopic cell is described in Sec. III F. One can easily see now that in order to build the field in a unit cell on a small cubic lattice $N=3$ it is enough to specify the values of the field $\phi(\mathbf{r})=\phi_{i,j,k}$ only at the points inside the tetrahedrons. The values of the field at the remaining points can be set by using the symmetry of the structures. Thus, instead of specifying $3^3=27$ values of $\phi_{i,j,k}$ one has to specify these values at four point of the cubic lattice for the simple cubic structure. Using this method in the case of double diamond structures gives even bigger gain, where it is sufficient to set the values of the field at five points in order to set up the field for a cubic lattice containing $5^3=125$ points.

The small lattice can be enlarged to the desired size by changing the number of points from N to $2N-1$ and finding the values of $\phi_{i,j,k}$ in new lattice sites by interpolation. The interpolation done to enlarge the lattice has no influence on the results. It may only speed up the calculations if it is done appropriately.

F. Symmetry

We impose on the field $\phi(\mathbf{r})$ the symmetry of the structure we are looking for by building up the field inside a unit cubic cell of a smaller polyhedron, replicating it by reflections, translations, and rotations. These polyhedra are pictured with thick solid lines in Figs. 6(a)–6(c). They are identical to the polyhedra described by Coxeter [37] as kaleidoscopic cells. Such a procedure not only guarantees that the field has required symmetry but also enables substantial reduction of independent variables $\phi_{i,j,k}$ in the function $F(\{\phi_{i,j,k}\})$.

The structures we have generated can be, in principle, characterized by space group symmetry [38,39,32], analogous to molecular crystals. The simple cubic structure has

the space group $Im\bar{3}m$, double diamond $F\bar{4}3m$, and gyroid $Ia3d$. However, this is not always obvious even for the structures of simple topology, which a Bravais lattice should be assigned to for a given structure [32]. For more complex structures, assigning a Bravais lattice becomes unclear. Therefore we decided to characterize the symmetry of the structures we have generated by including it in the class of symmetry characteristic for the following structures: simple cubic, double diamond, and gyroid. All these structures belong to the class of cubic symmetry; thus here we generate only the structures belonging to this class.

The structures having the symmetry of the simple cubic phase are built of a quadrirectangular tetrahedron replicating it by reflection [Fig. 6(a)]. The faces of the tetrahedron lie in the planes of mirror symmetry. The volume of the tetrahedron is $\frac{1}{48}$ of the unit cell volume.

The structures of the double diamond phase symmetry are built in the following way. First the unit cell is divided into eight smaller cubes. The field in the one of the small cubes is built of trirectangular tetrahedron in the same way as in the previous case [Fig. 6(b)]. The volume of the tetrahedron is $\frac{1}{24}$ of the unit cell volume. Next the field in the unit cell is built of this cube by translations and translations combined with a change of sign of the field from $\phi_{i,j,k}$ to $-\phi_{i,j,k}$. The cube with the field build of the tetrahedron is translated by the vectors $(L/2,L/2,0)$, $(0,L/2,L/2)$, and $(L/2,0,L/2)$. Next the sign of the field in the small cube is changed and the cube with such a different field is translated by the vectors $(0,0,L/2)$, $(0,L/2,0)$, $(L/2,0,0)$, and $(L/2,L/2,L/2)$. L in both cases is the unit cell length. Such a procedure enables the reduction of the unit cell volume by a factor $1/(8\times24)=\frac{1}{192}$.

If the $\phi(\mathbf{r}),-\phi(\mathbf{r})$ symmetry is not applied, the trirectangular tetrahedron can also be used to create the structures of double diamond phase symmetry. In such a case the cube shown in Fig. 6(b) as $\frac{1}{8}$ of the unit cell becomes the unit cell. The unit cell volume is therefore reduced by a factor $\frac{1}{24}$.

The structures of gyroid phase symmetry are built of a rectangular parallelopiped [Fig. 6(c)]. It consists $\frac{1}{16}$ of the unit cell volume. The parallelopiped is rotated by 90° according to a fourfold screw rotation axis parallel to the z direction, located at the point $\mathbf{r}=(L/4,L/4,L/4)$ and translated in the direction of the z axis by the vector $(L/4,0,0)$. Repeating this operation three times fills out $\frac{1}{4}$ of the unit cell volume with a new rectangular parallelopiped spanned by a vector $(L,L/2,L/2)$ located at the point $\mathbf{r}=(0,0,0)$. Next this new parallelopiped is rotated according to a twofold rotation axis parallel to the y direction and located at the point $\mathbf{r}=(L/2,0,L/2)$. The parallelopiped created by this operation spanned by the vector $(L,L/2,L/2)$ located at the point $\mathbf{r}=(L/2,0,0)$ is translated by the vector $(-L/2,L/2,0)$. The sign of the field in this parallelopiped is changed from $\phi_{i,j,k}$ to $-\phi_{i,j,k}$. After these transformation $\frac{1}{2}$ of the unit cell is recreated. The other half of the unit cell is created of the previous one by rotating it according to the twofold rotation axis parallel to the z direction and located at the point $\mathbf{r}=(L/2,L/2,0)$.

G. Accuracy of numerical computations

We use the conjugate gradient method [40] to minimize the function $F(\{\phi_{i,j,k}\})$. Minimization was done with respect to $\{\phi_{i,j,k}\}$ for a given value of the cell length $L=(N-1)h$. We have varied h to find the cell length for the lowest value of the function $F(\{\phi_{i,j,k}\})$.

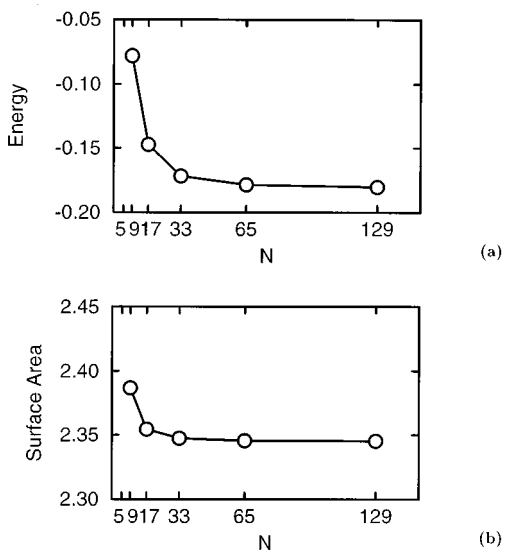

FIG. 7. (a) Free energy per unit volume and (b) normalized surface area per face of the unit cell of $\phi(\mathbf{r})=0$ for the simple cubic structure, calculated from the functional (2) for the parameters $f_0=0$ and $g_0=-3.0$ as a function of the lattice size.

The solution for the discretized model of a continuous functional is obtained with a certain accuracy. The accuracy depends on the value of the lattice spacing h and the number of points N. We have checked the accuracy of our results by calculating the free energy and the surface area of $\phi(\mathbf{r})=0$ for a few different sizes of the lattice. Figure 7(a) shows that the free energy is very sensitive for the lattice size. We used in our calculations $N=129$, which results in over 2×10^6 points per unit cell. This value seems to give sufficient accuracy for the calculation of the free energy. For the calculation of the surface area of $\phi(\mathbf{r})=0$ a smaller lattice can be used to obtain high accuracy. Figure 7(b) shows that the values of the surface area of the internal interface change only slightly for $N=33,65,129$.

IV. RESULTS

We have generated many unknown structures as well as a few known ones. Among the generated surfaces are the triply periodic minimal surfaces. These surfaces have been considered as paradigms of the internal interface in the ordered phases formed in the mixtures containing a surfactant. We describe these surfaces in Sec. IV A. To the best of our knowledge the results we present are the first ones showing that a triply periodic minimal surface can be the solution of a physical model. The surfaces of high genus are presented in Sec. IV B. The pictures of these surfaces strongly resemble the pictures of microemulsion taken during freeze fracture microscopy studies. In Sec. IV C we describe another type of structure, *the multiply continuous structure*. Our discovery calls for new experiments confirming or rejecting the existence of such structures in real systems (so far only bicontinuous structures have been considered). The phase diagram of the model is presented in Sec. IV D.

A. Minimal surfaces

The following simple experiment can be used for the direct visualization of a simple patch of minimal surface. Take a metal nonplanar frame and immerse it in a water solution of soap. The soap bubble that forms on this frame assumes the shape that minimizes its surface free energy associated with the surface tension and consequently it forms a surface of least area. Thus these surfaces are called minimal surfaces. Such experiments can be traced back to Leonardo da Vinci, but in fact detailed studies of this type were done and published by Plateau [41] and hence later the problem of a surface of least area spanning a given loop has been named the Plateau problem.

The history of physics and mathematics of minimal surfaces ran in parallel. Lagrange, in 1761 (before Plateau), derived equations for a surface of least area that are equivalent to the condition of vanishing mean curvature at every point on the surface. The representation of these surfaces in terms of harmonic functions was given by Weierstrass in 1866 and this representation has served many researchers up to date for their generations. Further qualitative insight into the mathematics of the problem was obtained by Schwarz and Neovius, who showed that simple patches of minimal surfaces can be put together to give smooth periodic three-dimensional structures, which are called now triply periodic minimal surfaces or sometimes infinite periodic minimal surfaces. They identified five phases, three of which were of cubic symmetry, i.e., P, D, and $C(P)$. Plateau and Schwarz in fact entertained scientific contacts, but none of them had envisaged the role of these surfaces as physical interfaces. The rediscovery of the problem is attributable to Schoen [39], who identified four surfaces of cubic symmetry (G, I-WP, F-RD, and O,C-TO). In 1976 Scriven [42] hypothesized that such surfaces could be used for the description of physical interfaces appearing in ternary mixtures of water, oil, and surfactants. In 1967–1968 Luzzati *et al.* [43–46] observed this type of ordering in the lecithin-water and lipid-water systems. One of the phases observed by them was the phase of the same symmetry as the G Schoen minimal surface. It seems that the discoveries of Schoen and Luzzati *et al.* were made independently. In fact, this phase appears to be very common in biological systems. Another example of such surfaces is found in the system of diblock copolymers, commercially important materials for the production of plastics. An AB diblock copolymer consists of two macromolecules chemically bonded together. At low temperatures the system forms ordered A-rich and B-rich domains, with the points of bondage at the interface between the domains. In 1988 Thomas *et al.* [47] observed that the polystyrene-polyisoprene (PS-PI) diblock copolymer forms a structure of the same symmetry as the D (diamond) Schwarz surface and argued on the basis of the relative volume fraction of PS and PI component that the resulting physical interface must be the surface of constant mean curvature at every point of the surface. Such a surface belongs to the family of minimal surfaces [39,32,48].

Surfaces are ubiquitous. Even in the ionic crystals one can imagine a periodic zero potential surface (POPS) having the same symmetry as the crystal [49]. Although POPSs do not usually have the same geometry as the minimal surfaces (their mean curvature varies along the surface), nonetheless they share the same topology (genus, etc.) and symmetry as the latter.

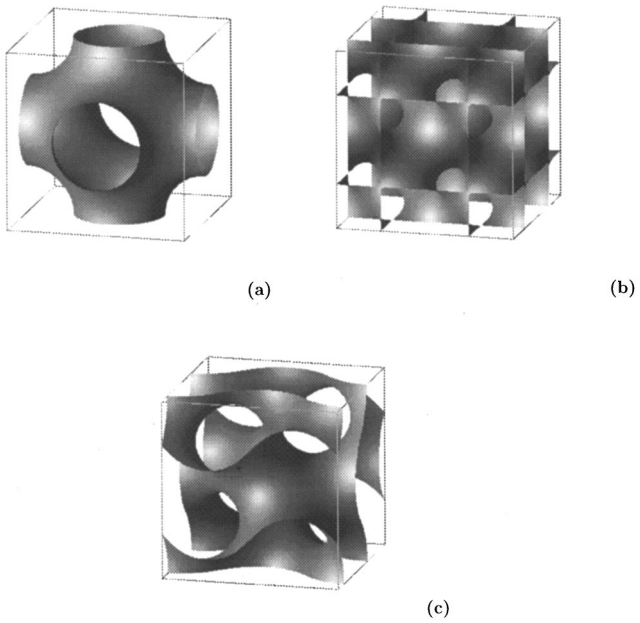

FIG. 8. Minimal surfaces generated from the functional (2): (a) Schwarz simple cubic P, (b) Schwarz diamond surface D, and (c) Schoen gyroid G. The unit cell is shown from an off front view.

The minimal surfaces are usually described in terms of Weierstrass integral equations. The Weierstrass representation gives the coordinates (x,y,z) on a minimal surface of the point represented by ω in the complex plane [50]

$$x=\mathrm{Re}\int_{\omega_0}^{\omega_1}(1-\omega^2)R(\omega)d\omega,$$

$$y=\mathrm{Re}\int_{\omega_0}^{\omega_1}i(1+\omega^2)R(\omega)d\omega,$$

$$z=\mathrm{Re}\int_{\omega_0}^{\omega_1}2\omega R(\omega)d\omega, \tag{24}$$

where $R(\omega)$ is the Weierstrass characteristic function for the surface, Re stands for the ''real part,'' $\omega=\omega_a+i\omega_b$, and $i=\sqrt{-1}$. When the function $R(\omega)$ is replaced with $R(\omega)e^{i\theta}$ the surface described by the function $R(\omega)$ is transformed into another surface called the adjoint surface. Such a transformation is called the Bonnet transformation [51] and θ is known as the Bonnet angle. The Bonnet transformation preserves the Gaussian and mean curvatures.

1. Schwarz surfaces D,P and Schoen surface G

The Schwarz primitive surface P [Fig. 8(a)] and Schoen gyroid surface G [Fig. 8(c)] are related to the D surface [Fig. 8(b)] by the Bonnet transformation: the Bonnet angle for the P surface is 90° and for the G surface it is 38.015°. The Weierstrass function for the fundamental element of the surfaces D is given by [50,52]

$$R(\omega)=(\omega^8-14\omega^4+1)^{-1/2}, \tag{25}$$

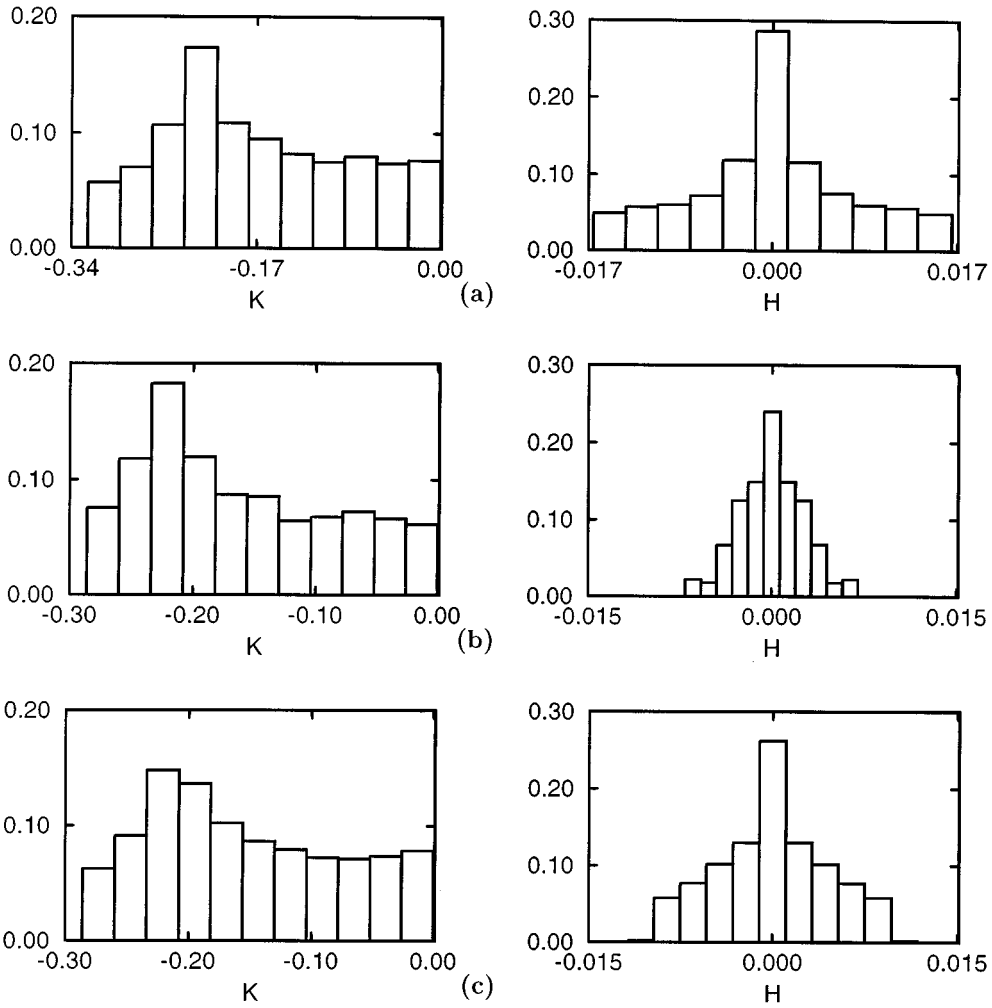

FIG. 9. Histograms of the Gaussian (K) and mean (H) curvature for the surface: (a) Schwarz P, (b) Schwarz D, and (c) Schoen G.

with an integration domain given by the points around the origin limited by four circles with radius $\sqrt{2}$ and centers at $\pm\sqrt{2}, \pm i\sqrt{2}$.

Here we use our model to generate surfaces. The fact that the P,D,G (see Fig. 8) surfaces are adjoint means that the histograms of the Gaussian curvature for these surfaces should be the same. In fact, the histograms look very similar (see Fig. 9); the small differences result from the numerical accuracy. The mean curvature of the minimal surface is zero at every point; thus its histogram should be a single infinitely sharp peak at $H=0$. Here it is smeared (see Fig. 9) due to numerical accuracy. In fact, it serves as a good estimate of the errors for curvatures.

It is interesting that the value of the free energy in our model (2) for each of these structures is the lowest for all the structures of given symmetry, i.e., among all structures of the symmetry of gyroid phase G, this phase has the lowest free energy. These phases are generated independently of the initial configuration, provided that the unit cell length is set close to the minimal length. If the cell length is taken close to multiple length of the unit cell then multiple images of a given structure are formed.

The fact that the G and D structures are the most stable among the structures of a given symmetry suggest that they can be found in real systems. In fact, the phases diamond D and gyroid G have been discovered in real systems in diblock copolymers [47,53–56]. However, the discovery of the gyroid phase, after the diamond phase had been found in real systems, was not straightforward. It took the researchers about six years after the discovery of D phase to find the gyroid phase in the PI-PS system of diblock copolymers. Recent studies [57] show that the diamond phase in diblock copolymer systems is not stable. The only stable one is the gyroid phase. This is in accord with our calculations where the free-energy value for the gyroid phase is smaller than for the diamond phase.

2. Schoen I-WP and O,C-TO minimal surface

The I-WP surface [Fig. 10(a)] was discovered by Schoen [39]. He built the models of the surface, and identified its space group as $Im3m$. That is why the letter I is in the first part of the name given by him to this surface. The WP stands for ''wrapped package'' because of the resemblance of finite portions of the graph to the arrangement of string on a simply wrapped package. The Weierstrass characteristic function for the I-WP surface is [51,58]

$$R(\omega)=(\omega^6-5\omega^4-5\omega^2+1)^{-2/3}. \tag{26}$$

The I-WP surface was found in star block copolymers [59].

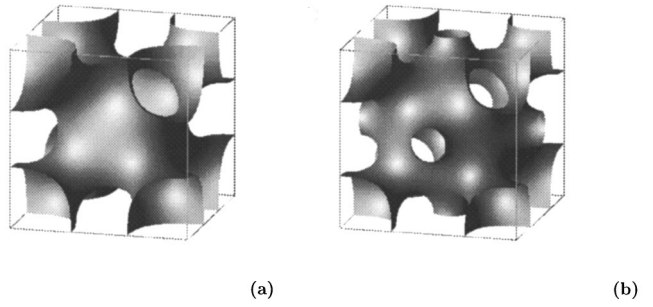

FIG. 10. Schoen minimal surfaces generated from the functional (2): (a) *I*-WP and (b) *O,C-TO*. The unit cell is shown from an off front view.

The results of our study suggest that it can also be found in the ternary surfactant mixtures.

The *O,C-TO* surface [Fig. 10(b)] was discovered by Schoen [39]. The Weierstrass function for this surface is not known and no other information except the genus and the symmetry are described in the literature. Here we report the volume fraction of the two subvolumes divided by the *O,C-TO* surface; see Table I. As far as we know, nobody so far has shown the existence of this structure in real systems. The surface obtained from the functional (2) strongly resembles the one described by Schoen. The histogram of the mean curvature suggests that this surface can be minimal. However, this is the only structure that cannot be minimized with respect to the cell length. For all structures except this one we were able to find the minimal cell length, i.e., varying the cell length we were able to find such a length for which the free-energy density of the functional (2) is minimal. The *O,C-TO* structure collapses to *I*-WP when the cell length is varied. Such a behavior suggests that this structure is very unstable and finding it in real systems is problematic.

It should be pointed out here that although the free energy depends on the cell length, the geometric properties of the surface $\phi(\mathbf{r})=0$ do not. The surface area per face of the unit cell $\tilde{S}$ is the same, for a given structure, at different points of the phase diagram and for different values of the cell length. The free energy depends on the three-dimensional scalar field $\phi(\mathbf{r})$ and that is why it varies for different values of the cell length and for different points on the phase diagram. However, $\tilde{S}$ and the mean curvature $H(\mathbf{r})$ for the surface $\phi(\mathbf{r})=0$ are scale invariant.

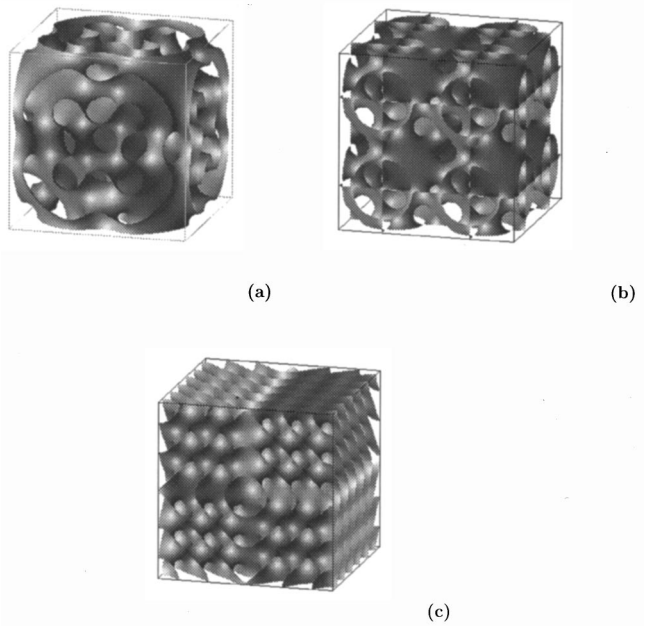

FIG. 11. High-genus surfaces generated from the functional (2): (a) the surface *SCN*1 of symmetry of the *P* surface [see Fig. 8(a)], (b) the surface *CD* of symmetry of the *D* surface [see Fig. 8(b)], (c) the surface *GX*5 of symmetry of the *G* surface [see Fig. 8(c)]. The unit cell is shown from an off front view.

B. High-genus embedded periodic surfaces

The high-genus surfaces are most easily generated for the values of parameters f_0 and g_0 in (2) taken near the boundary of lamellar and microemulsion phase and for a larger unit cell length $L=(N-1)h$ than the length of structures of low genus. This suggests that the microemulsion can be considered as a bicontinuous structure of the high-genus surface. These are only speculations based upon theoretical studies. New experiments are needed to check these speculations. We hope that our results will help experimentalists design such experiments.

TABLE I. Geometrical properties of the known minimal surfaces obtained from the functional (2), for the parameters $f_0=0.0$ and $g_0=-3.0$. The exact values found in the literature are given in square brackets. The surface area $\tilde{S}$ is the normalized per face of the unit cube L^2 surface area S of the interface in the unit cell $\tilde{S}=S/L^2$ and $L=(N-1)h$. The energy is given per unit volume.

Name	Cell length	Energy	Surface area	Genus	Volume fraction
P	7.88	−0.181	2.3453 [2.345 106 8]	3	0.5
D	12.56	−0.188	3.8387 [3.837 786 2]	9	0.5
I-WP	11.78	−0.180	3.4640 [3.464 601 6]	7	0.533
G	10.08	−0.190	3.0919	5	0.5
O,C-TO	14.68	−0.162	3.6805	10	0.535

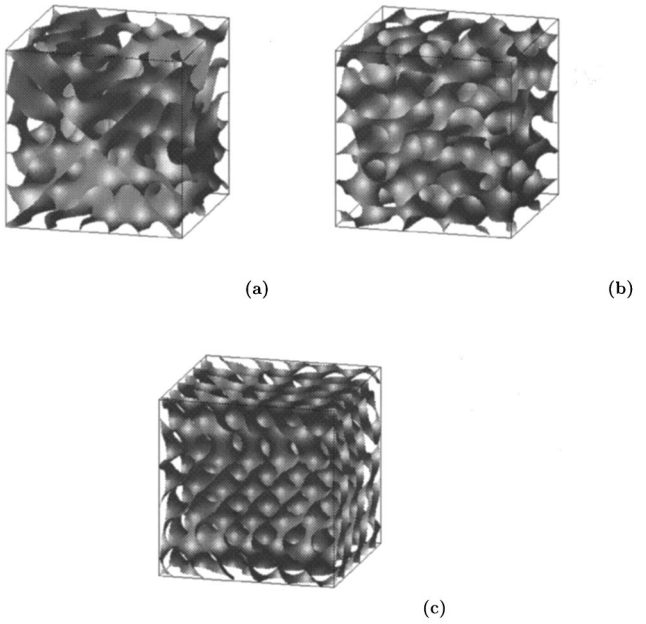

FIG. 12. High-genus gyroid surfaces generated from the functional (2): (a) *GX*1, (b) *GX*2, and (c) *GX*3. The unit cell is shown from an off front view.

We present in this section several examples of high-genus surfaces of different symmetry. The structure *SCN*1 [Fig. 11(a)] has the symmetry of the simple cubic phase [Fig. 8(a)], the structure *CD* [Fig. 11(b)] has the symmetry of double diamond phase [Fig. 8(b)], and the structures *GX*5 [Fig. 11(c)], *GX*1 [Fig. 12(a)], *GX*2 [Fig. 12(b)], and *GX*3 [Fig. 12(c)] have the gyroid phase [Fig. 8(c)] symmetry, see also [60].

The *SCN*1 surface [Fig. 11(a)] is similar to the *BFY* surface [29], but because its unit cell length is larger, the surface is more complex. A comparison of these surfaces can be used as an example of how the functional (2) keeps the size of the water and oil regions the same for different structures. For a bigger cell length the surface dividing the oil and water regions is folded a few times in order to keep the sizes of the oil and water regions resulted from the functional (2) for given values of the parameters f_0, g_0.

The *CD* [Fig. 11(b)] structure is especially interesting because it has the same symmetry as the Schwartz diamond *D* phase. It has been generated in the same way as the diamond *D* phase, that is, we have reduced the unit cell by a factor $\frac{1}{192}$. Having done such a reduction, we hardly expected the possibility of the generation of a new surface. In fact, enlarging

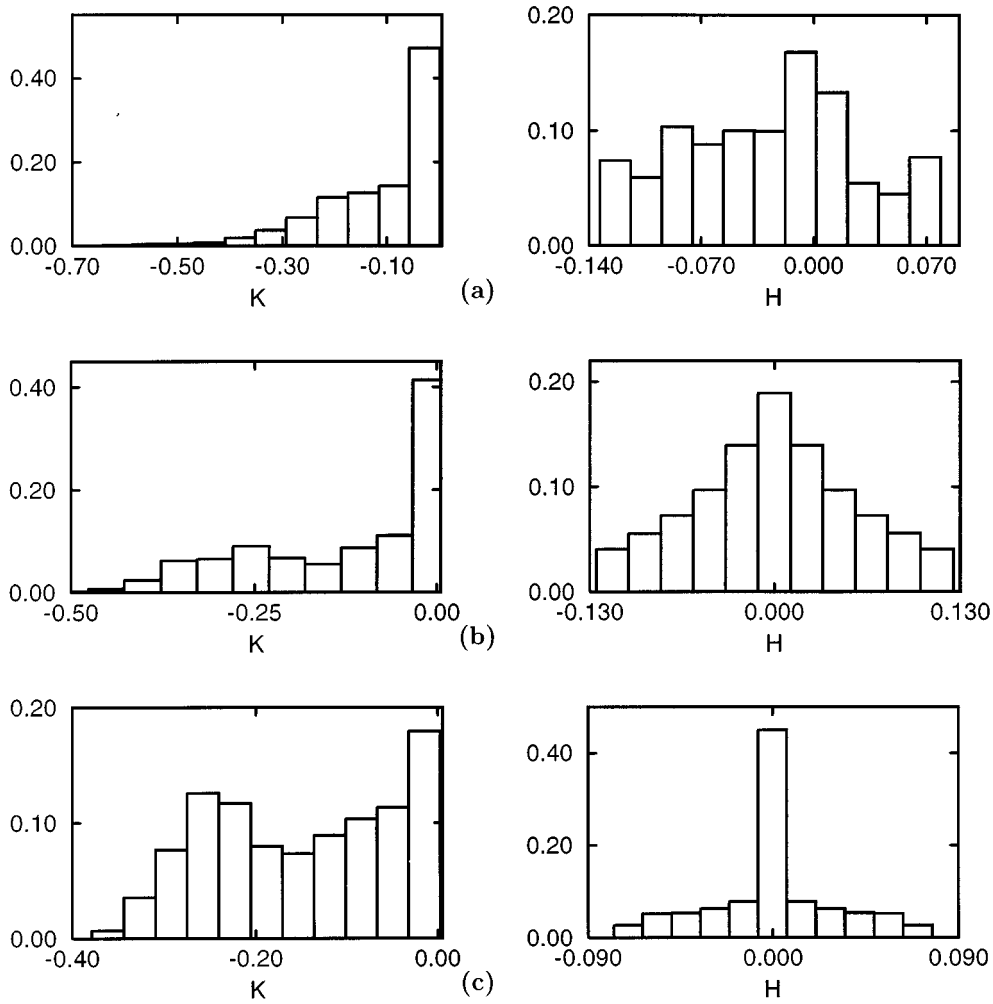

FIG. 13. Histograms of the Gaussian (K) and mean (H) curvature for the surface: (a) *SCN*1 [Fig. 8(a)], (b) *CD* [Fig. 8(b)], and (c) *GX*5 [Fig. 8(c)].

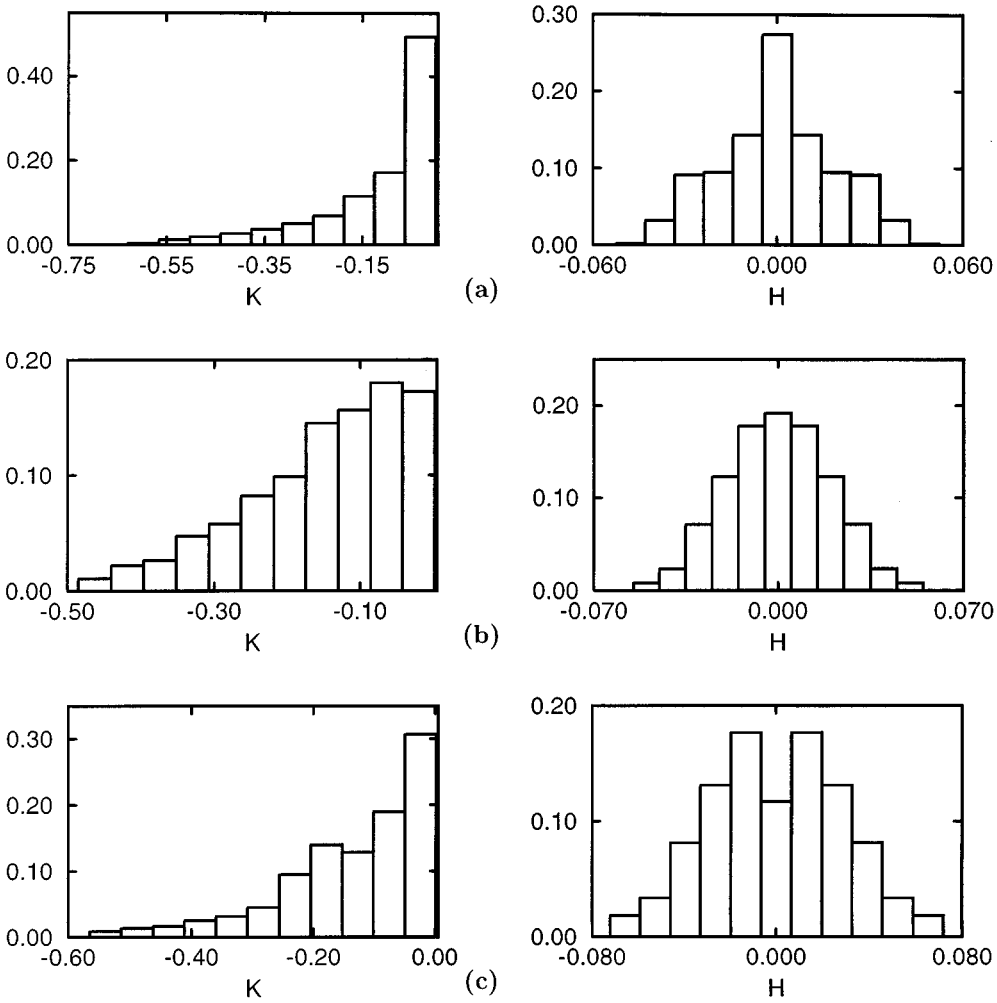

FIG. 14. Histograms of the Gaussian (K) and mean (H) curvature for the surface: (a) $GX1$ [Fig. 12(a)], (b) $GX2$ [Fig. 12(b)], and (c) $GX3$ [Fig. 12(c)].

the length of the cubic cell, we usually obtained the multiple replicas of the diamond D structure, except for the case when the CD structure was generated.

We have generated high-genus surfaces of vanishing curvatures; see Figs. 13 and 14. The existence of such surfaces in real systems was questioned. The researches argued that it is impossible to build high-genus periodic surfaces because of large curvatures, which could not be accommodated by the displacement of surfactant molecules at the surface [61]. As we can see from Table II, high-genus surfaces have large unit cells and therefore their curvatures (see the Gaussian curvatures) are similar in magnitude to those of surfaces of low genus. Therefore the argument against the existence of these surfaces does not hold.

The pictures of the high-genus structures, especially the gyroid ones, strongly resemble the pictures of microemulsion taken during freeze fracture microscopy studies [5,8]. The gyroid high-genus surfaces have in general lower free energy than the surfaces of other symmetries. We can speculate that this symmetry would be preferred in real systems. In fact, the Schoen gyroid G minimal surface is the most common in nature among the known minimal surfaces. The gyroid surfaces do not have planes of symmetry. This may cause easier adaptation of their shape to the structures encountered in nature, such as diblock copolymers, lipid-water solutions, or surfactant mixtures.

The properties of high-genus surfaces are calculated with lower accuracy than the properties of those of low genus.

TABLE II. Geometrical properties of high-genus surfaces obtained from the functional (2), for the parameters $f_0=0.0$ and $g_0=-3.0$. The surface area $\tilde{S}$ is the normalized per face of the unit cube L^2 surface area S of the interface in the unit cell $\tilde{S}=S/L^2$ and $L=(N-1)h$. The energy is given per unit volume. The volume fraction for all structures is 0.5.

Name	Cell length	Energy	Surface area	Genus
$SCN1$	25.6	−0.178	7.4288	45
CD	28.88	−0.167	8.2257	73
$GX1$	26.16	−0.186	7.907	53
$GX2$	26.48	−0.183	8.081	69
$GX3$	31.72	−0.181	9.657	109
$GX5$	34.40	−0.178	10.519	157

This is so because we have used the same size of the lattice N for the unit cell. This results in a bigger lattice spacing h. For high-genus structures more surface has to be accommodated in the unit cell; therefore the calculation of the derivatives is less accurate.

The biggest errors are in calculations of the curvatures because all possible approximations are accommodated in these calculations. First is the approximation used to find the surface $\phi(\mathbf{r})=0$. The location of this surface has to be linearly interpolated between the lattice sites. The formulas for the mean and Gaussian curvature are also numerical approximations of the analytic expressions. The derivatives used in calculations are also numerical approximations. The points used to calculate the derivatives have to be interpolated between the lattice sites. Finally, the discretization and minimization of the functional also introduces some errors. It is amazing that, in spite of all those sources of errors, the curvatures are calculated with such a high accuracy, which can be seen by looking at the histograms of the mean curvature for P,D,G minimal surfaces; see Fig. 9.

C. Multiply continuous embedded periodic surfaces

The possibility of the existence of multiply continuous structures in ternary mixtures of oil water and surfactant has not been discussed so far (see, however, the paper on triblock copolymers [62]). In the bicontinuous structure the single surface separates the volume into two disjoint subvolumes. In our phases there is more than one periodic surface that disconnects the volume into three or more disjoint subvolumes. The multiply continuous structures are most easily generated for the values of parameters f_0 and g_0 in (2) taken near the boundary of lamellar and water (oil) phase and for the bigger unit cell length $L=(N-1)h$ than the length of structures of low genus. The experimental results do not rule out the existence of such structures; contrarily, the experiment on the electrical conductivity supports the idea [5,6]. It would be very interesting to design an experiment answering the question whether the structures considered so far as bicontinuous are only bicontinuous or maybe multiply continuous.

We present the multiply continuous structures of the simple cubic phase symmetry (*SCL*1 and *SCL*2 in Fig. 15) and of the gyroid phase symmetry (*GL*1 and *GL*2 in Fig. 16). The *SCL*1 structure is triply continuous, the *GL*1 and *SCL*2 are quadruply continuous, and *GL*2 is sixtuply continuous. For bigger unit cells one is able to generate the structures n-tuply continuous. It is remarkable that the volume fraction of oil and water is 0.5 for all these structures. The genera for all surfaces in a given structure are the same. Other properties of the multiply continuous structures are described in Table III.

The *SCL*1 surface is especially interesting. Although the outer and the inner surface look different in Fig. 15(a), they have the same surface area; see Table III. In fact, they are built of the same piece of the surface. The picture of $\frac{1}{8}$ of the unit cell [see Fig. 15(b)] explains how two different periodic surfaces can be built of the same surface patch.

The *SCL*2 structure is composed of three different embedded periodic surfaces [Fig. 15(c)]. The middle surface is the Schwarz minimal surface P and its normalized surface area

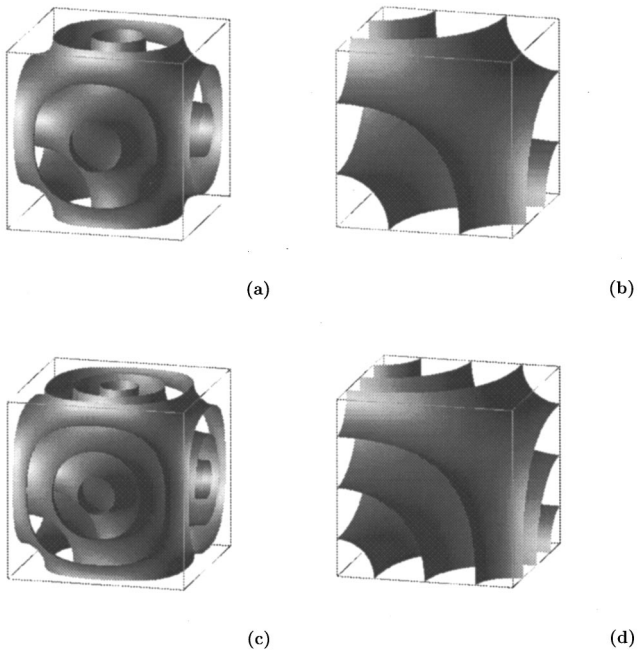

FIG. 15. Multiply continuous structures of symmetry of the simple cubic phase [see Fig. 8(a)], generated from the functional (2): (a) the unit cell of the *SCL*1 triply continuous structure, (b) $\frac{1}{8}$ of the unit cell of the *SCL*1 structure, (c) the unit cell of *SCL*2 quadruply continuous structure, and (d) $\frac{1}{8}$ of the unit cell of *SCL*2 structure. The unit cell is shown from an off front view.

of these surfaces is the same within the numerical errors; see Tables III and I. Similarly, the middle phase surface in *GL*1 [Fig. 16(a)] and *GL*2 [Fig. 16(b)] structures is the Schoen minimal surface G; see Tables III and I.

The *GL*2 structure suggests that one can generate arbitrary n-tuply continuous structures. It is only necessary to set the cell length sufficiently large. We have not attempted generation of such structures because, due to the limits imposed by computer memory and the speed of the processor, the lattice spacing would be too big for a given size of the lattice to obtain reasonable accuracy.

D. Stability of different phases in the model

We have investigated many bicontinuous phases of different symmetries, genera, and dimensions of the unit cell. The

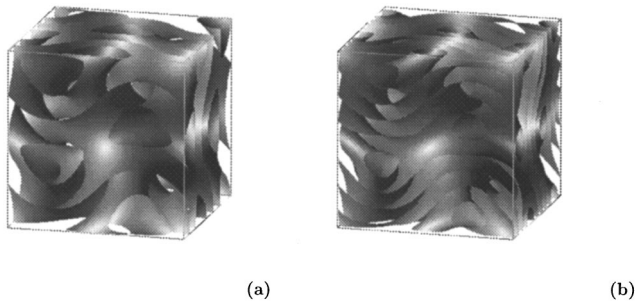

FIG. 16. Multiply continuous structures of symmetry of the gyroid phase [see Fig. 8(c)], generated from the functional (2): (a) the unit cell of quadruply continuous *GL*1 structure and (b) the unit cell of sixtuply continuous *GL*2 structure. The unit cell is shown from an off front view.

TABLE III. Geometrical properties of multiply continuous structures obtained from the functional (2), for the parameters $f_0=0.0$ and $g_0=-3.0$. The surface area $\tilde{S}$ is the normalized per face of the unit cube L^2 surface area S of the interface in the unit cell $\tilde{S}=S/L^2$ and $L=(N-1)h$. The energy is given per unit volume. The volume fraction for all surfaces is 0.5. The genus is given for any single surface in the structure.

Name	Cell length	Energy	Surface area	Genus
*SCL*1	14.96	−0.175	4.090	3
1			2.045	
2			2.045	
*SCL*2	21.14	−0.178	5.780	3
1			1.716	
2			2.348	
3			1.716	
*GL*1	26.32	−0.187	7.546	5
1			2.226	
2			3.096	
3			2.226	
*GL*2	41.16	−0.185	11.887	5
1			1.659	
2			2.736	
3			3.097	
4			2.736	
5			1.659	

bicontinuous phase with the lowest value of the free energy turned out to be the gyroid, but the only stable liquid crystalline phase in this model is the lamellar phase. Figure 17 shows the plot of the free energy as a function of the parameter f_0 for the lamellar and gyroid phases. The phase diagram for the model (2), in the mean-field approximation, calculated by Gompper and Zschocke [22] and checked here is shown in Fig. 18. Other bicontinuous phases behave in the same way as the gyroid and lamellar. The value of the free energy in the vicinity of microemulsion boundary converges to the value of the free energy for the microemulsion. The geometric characteristics such as genus and normalized surface area are the same for all phases in different places of the phase diagram.

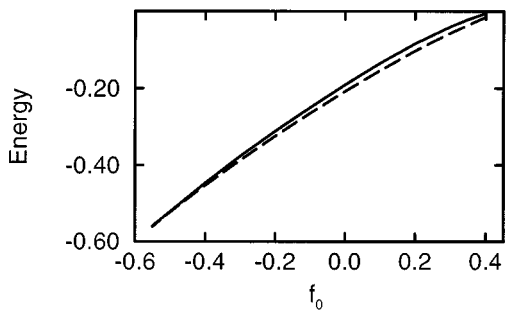

FIG. 17. Free energy per unit volume for the lamellar phase (dashed line) and gyroid phase (solid line) for the model (2). The parameter $g_0=-3.0$.

We have also studied the stability of bicontinuous phases for different functions describing the surfactant $g(\phi(\mathbf{r}))$. We have used the following form of $g(\phi(\mathbf{r}))$:

$$g(\phi(\mathbf{r}))=g_2\phi(\mathbf{r})^4+g_0. \tag{27}$$

We have expected that this form of $g(\phi(\mathbf{r}))$ would make the interface between oil and water sharper and therefore it would lower the free energy. The interface indeed was sharper as we expected, but the unit cell length decreased also. This resulted in higher values of the free energy than before and all bicontinuous phases were metastable as in the previous case. It might suggest that one order parameter functional is not sufficient to describe the behavior of ordered phases. We note that in the case of multiparameter Landau models introduced in recent years [5] we may expect the stabilization of the various phases that in the one order parameter Landau model are only metastable [26]. Our current results are a very good starting point for the investigation of the stability of bicontinuous phases in multiparameter Landau functionals.

V. CONCLUSION

It is amazing that the solutions of the physical model of microemulsion can be triply periodic minimal surfaces. So far the triply periodic minimal surfaces were generated from the Weirstrass representation or from the definition of the mean curvature. For over 100 years mathematicians have discovered a few infinite embedded periodic minimal surfaces of cubic symmetry.

We found that the surfaces generated from the functional (2) are triply periodic surfaces of nonpositive Gaussian curvature. Some of them may be new minimal surfaces. Especially interesting are the surfaces of high genus. The existence of such surfaces may suggest that microemulsion can be the structure with such a surface of very high genus.

We have discovered multiply continuous cubic structures formed in ternary mixtures of water, oil, and surfactant. The idea of multiple continuity of cubic structures is different. Our results call for new experimental techniques that could be used to discern between bicontinuous and multiply continuous structures. We hope that these new structures will soon be discovered in real systems.

We have not only calculated the properties of many cubic structures and investigated their stability, but also presented the pictures of new structures. We hope that this will help other workers better understand the phenomena in ternary liquid mixtures, diblock copolymers, and biological systems.

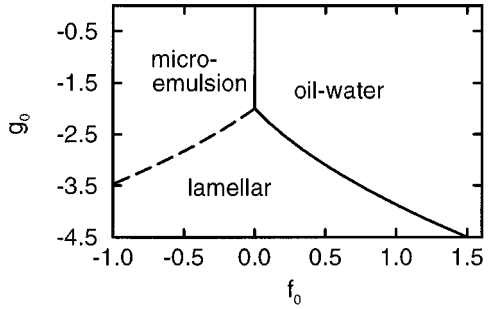

FIG. 18. Phase diagram for the model (2).

We have presented the general method for the generation of periodic surfaces of nonpositive Gaussian curvature. This method can be well applied by physicists working in soft condensed matter, mathematicians working in topology, biologists, and crystallographers. Certainly the richness of the method is far from being completely explored by our work.

Our results are also an ideal starting point, for theoreticians, to pursue the studies of Landau-Ginzburg models with more than one order parameter field [26], to investigate dynamical properties of complex systems [63,64], or to study complex fluids in confined geometries [23]. These are only a few benefits of this work and this is not a complete list.

Note added. We would like to thank Dr. Veit Elser for sending us a copy of his work on quasicrystalline minimal surfaces [65]. He has obtained minimal surfaces from a similar model of the free-energy functional.

ACKNOWLEDGMENTS

This work was supported by Komitet Badań Naukowych, Grants Nos. 2P30302007 and 2P03B01810. We also acknowledge support from Fundacja Współpracy Polsko-Niemieckiej.

[1] R. G. Laughlin, *The Aqueous Phase Behavior of Surfactants* (Academic, London, 1994).
[2] *Physics of Amphiphiles: Micelles, Vesicles and Microemulsions*, edited by V. Degiorgio and M. Corti (North-Holland, Amsterdam, 1985).
[3] M. Kalhweit *et al.*, J. Colloid Interface Sci. **118**, 436 (1987).
[4] M. Kahlweit *et al.*, Langmuir **4**, 499 (1988).
[5] G. Gompper and M. Schick, *Phase Transitions and Critical Phenomena*, 1st ed. (Academic, New York, 1994), Vol. 16.
[6] A. Ciach, Pol. J. Chem. **66**, 1347 (1992).
[7] K. V. Schubert and R. Strey, J. Chem. Phys. **95**, 8532 (1991).
[8] W. Jahn and R. Strey, J. Phys. Chem. **92**, 2294 (1988).
[9] A. Ciach, J. Chem. Phys. **96**, 1399 (1992).
[10] A. Ciach and A. Poniewierski, Phys. Rev. E **52**, 596 (1995).
[11] H. Chung and M. Caffrey, Nature **368**, 224 (1994).
[12] Z. Gang Wang and S. A. Safran, Europhys. Lett. **11**, 425 (1990).
[13] R. Lipowsky, Nature **349**, 475 (1991).
[14] W. Helfrich, Z. Naturforsch. Teil. A **28**, 693 (1973).
[15] L. D. Landau and E. M. Lifshitz, *Statistical Physics*, 3rd ed. (Pergamon, New York, 1989).
[16] M. Teubner and R. Strey, J. Chem. Phys. **87**, 3195 (1987).
[17] G. Gompper and M. Schick, Phys. Rev. Lett. **65**, 1116 (1990).
[18] G. Gompper, R. Hołyst, and M. Schick, Phys. Rev. A **43**, 3157 (1991).
[19] J. Putz, R. Hołyst, and M. Schick, Phys. Rev. A **46**, 3369 (1992), Phys. Rev. E **46**, 3035 (1993).
[20] G. Gompper and M. Hennes, J. Chem. Phys. **102**, 2871 (1994).
[21] G. Gompper and S. Zschocke, Europhys. Lett. **16**, 731 (1991).
[22] G. Gompper and S. Zschocke, Phys. Rev. A **46**, 4836 (1992).
[23] F. Schmid and M. Schick, Phys. Rev. E **48**, 1882 (1993).
[24] G. Gompper and J. Goos, Phys. Rev. E **50**, 1325 (1994).
[25] M. Laradji, H. Guo, M. Grant, and M. J. Zuckermann, Phys. Rev. A **44**, 8184 (1991).
[26] A. Ciach, J. Chem. Phys. **104**, 2376 (1996).
[27] K. Kawasaki and T. Kawakatsu, Physica A **164**, 549 (1990).
[28] G. Gompper and S. Klein, J. Phys. (France) II **2**, 1725 (1992).
[29] W. Góźdź and R. Hołyst, Macromol. Theory Simul. **5**, 321 (1996).
[30] *Handbook of Mathematical Functions With Formulas, Graphs, and Mathematical Tables*, 9th ed. Nat. Bur. Stand. Appl. Math. Ser. No. 55, edited by M. Abramowitz and I. A. Stegun (U.S. GPO, Washington, DC, 1970), pp. 883 and 884.
[31] D. A. Hoffman, J. Phys. (Paris) Colloq. **51**, C7-197 (1990).
[32] D. M. Anderson, H. T. Davis, L. E. Scriven, and J. C. C. Nitsche, Adv. Chem. Phys. **77**, 337 (1990).
[33] S. T. Hyde, Z. Kristallogr. **187**, 165 (1989).
[34] I. S. Barnes, S. T. Hyde, and B. W. Ninham, J. Phys. (Paris) Colloq. **51**, C7-19 (1990).
[35] A. L. Mackay and J. Klimowski, Comput. Math. Appl. B **12**, 803 (1986).
[36] M. Spivak, *A Comprehensive Introduction to Differential Geometry* (Publish or Perish, Berkeley, 1979), Vol. III.
[37] H. Coxeter, *Regular Polytopes* (MacMillan, New York, 1963).
[38] *International Tables for X-Ray Crystallography*, edited by N. S. M. Henry and K. Lonsdale (Kynoch, Birmingham, England, 1952), Vol. 1.
[39] A. H. Schoen, NASA Report No. TN D-5541, 1970 (unpublished).
[40] W. H. Press, B. P. Flannery, S. A. Teukolsky, and W. T. Vetterling, *Numerical Recipes* (Cambridge University Press, Cambridge, 1990).
[41] J. A. F. Plateau, *Statique Expérimentale et Théorique des Liquides aux Seules Forces Moléculaires* (Gauthier-Villars, Paris, 1873), Vol. 2.
[42] L. E. Scriven, Nature **263**, 123 (1976).
[43] V. Luzzati and P. A. Spegt, Nature **215**, 701 (1967).
[44] V. Luzzati, A. Tardieu, and T. Gulik-Krzywicki, Nature **217**, 1028 (1968).
[45] V. Luzzati, T. Gulik-Krzywicki, and A. Tardieu, Nature **218**, 1031 (1968).
[46] V. Luzzati, A. Tardieu, T. Gulik-Krzywicki, E. Rivas, and F. Reiss-Husson, Nature **220**, 485 (1968).
[47] E. L. Thomas, D. M. Anderson, C. Henkee, and D. Hofman, Nature **334**, 598 (1988).
[48] A. L. Mackay, Nature **314**, 604 (1985).
[49] H. G. von Schnering and R. Nesper, Angew. Chem., Int. Ed. Engl. **26**, 1059 (1987).
[50] H. Terrones, J. Phys. (Paris) Colloq. **51**, C7-345 (1990).
[51] S. Lidin, S. T. Hyde, and B. W. Ninham, J. Phys. (Paris) **51**, 801 (1990).
[52] A. Fodgen, J. Phys. (Paris) Colloq. **51**, C7-149 (1990).
[53] E. L. Thomas, D. B. Alward, D. J. Kinning, D. C. Martin, and L. J. Fetters, Macromolecules **19**, 2187 (1986).
[54] H. Hasegawa, H. Tanaka, K. Yamasaki, and T. Hashimoto, Macromolecules **20**, 1651 (1986).
[55] D. J. Kinning, J. M. Ottino, and E. Thomas, Macromolecules **20**, 1129 (1986).

[56] D. A. Hajduk *et al.*, Macromolecules **27**, 4063 (1994).
[57] D. A. Hajduk *et al.*, Macromolecules **28**, 2570 (1995).
[58] D. Cvijović and J. Klimowski, Chem. Phys. Lett. **226**, 93 (1994).
[59] D. M. Anderson, Ph.D. thesis, University of Minnesota, 1986 (unpublished).
[60] W. Góźdź and R. Hołyst, Phys. Rev. Lett. **76**, 2726 (1996).
[61] S. T. Hyde, J. Phys. Chem. **93**, 1458 (1989).
[62] Y. Mogi, K. Mori, Y. Kaneko, K. Mori, and Y. Matsushita, Macromolecules **25**, 5408 (1992).
[63] G. Gompper and M. Hennes, Europhys. Lett. **25**, 193 (1994).
[64] G. Gompper and M. Hennes, Phys. Rev. Lett. **73**, 1114 (1994).
[65] Q. Sheng and V. Elser, Phys. Rev. B **49**, 9977 (1994).